Impact of a novel hybrid accelerometer on satellite gravimetry performance

Petro Abrykosov, Roland Pail, Thomas Gruber, Nassim Zahzam, Alexandre Bresson, Emilie Hardy, Bruno Christophe, Yannick Bidel, Olivier Carraz, Christian Siemes

Impact of a novel hybrid accelerometer on satellite gravimetry performance

Petro Abrykosov* (petro.abrykosov@tum.de), Roland Pail (roland.pail@tum.de), Thomas Gruber (thomas.gruber@tum.de)
Lehrstuhl für Astronomische und Physikalische Geodäsie, Technische Universität München, Arcisstraße 21, 80333 München, Germany

Nassim Zahzam (nassim.zahzam@onera.fr), Alexandre Bresson (Alexandre.Bresson@onera.fr), Emilie Hardy (Emilie.Hardy@onera.fr), Bruno Christophe (bruno.christophe@onera.fr), Yannick Bidel (Yannick.Bidel@onera.fr)
DPHY, ONERA, Université Paris-Saclay, Chemin de la Hunière - BP 80100, F-91123 Palaiseau, France

Olivier Carraz (olivier.carraz@esa.int), Christian Siemes (christian.siemes@esa.int)
RHEA for ESA - European Space Agency, Keplerlaan 1, P.O. Box 299, 2200 AG Noordwijk, The Netherlands

Abstract

The state-of-the-art electrostatic accelerometers (EA) used for the retrieval of non-gravitational forces acting on a satellite constitute a core component of every dedicated gravity field mission. However, due to their difficult-to-control thermal drift in the low observation frequencies, they are also one of the most limiting factors of the achievable performance of gravity recovery. Recently, a hybrid accelerometer consisting of a regular EA and a novel cold atom interferometer (CAI) that features a time-invariant observation stability and constantly recalibrates the EA has been developed in order to remedy this major drawback. In this paper we aim to assess the value of the hybrid accelerometer for gravity field retrieval in the context of GRACE-type and Bender-type missions by means of numerical closed-loop simulations where possible noise specifications of the novel instrument are considered and different components of the Earth's gravity field signal are added subsequently. It is shown that the quality of the gravity field solutions is mainly dependent on the CAI's measurement accuracy. While a low CAI performance (10^{-8} to 10^{-9} m/s^2/Hz$^{1/2}$) does not lead to any gains compared to a stand-alone EA, a sufficiently high one (10^{-11} m/s^2/Hz$^{1/2}$) may improve the retrieval performance by over one order of magnitude. We also show that improvements which are limited to low-frequency observations may even propagate into high spherical harmonic degrees. Further, the accelerometer performance seems to play a less prominent role if the overall observation geometry is improved as it is the case for a Bender-type mission. The impact of the accelerometer measurements diminishes further when temporal variations of the gravity field are introduced, pointing out the need for proper de-aliasing techniques. An additional study reveals that the hybrid accelerometer is – contrary to a stand-alone EA – widely unaffected by scale factor instabilities.

Keywords: gravity field, numerical simulations, accelerometry, hybrid accelerometer, cold atom gravimeter, next generation gravity mission

* Corresponding author
Email address: petro.abrykosov@tum.de, Tel.: +49 89 289 231 85

1 Introduction

Climate change is one of the biggest societal challenges today. Understanding the underlying processes, which are most frequently related to mass variations in the Earth system, is a prerequisite for climate modelling and forecast. As changes in gravity are directly related to mass variability, satellite missions observing the Earth's time varying gravity field are a unique tool for observing mass redistribution among the Earth's system components including global changes in the water cycle, the cryosphere and the oceans. These observations provide essential indicators of both subtle and dramatic global change and are complementary to many other Earth observation technologies and missions. We have gained essential experience in observing the Earth's gravity field via the successful GRACE (Tapley et al., 2004) and GOCE (Drinkwater et al., 2003) missions, the former currently being extended through the successfully launched GRACE Follow-On mission (Flechtner et al., 2018). The need for sustained observation of mass transport from space was expressed by a resolution adopted by the Council of the International Union of Geodesy and Geophysics (IUGG, 2016). Besides requesting higher spatial resolution in order to allow for more regional applications, it was in particular the need for long and consistent time series that has been expressed by an international expert panel under the umbrella of IUGG representing all relevant geoscientific applications (Pail et al., 2015).

Therefore, currently several concepts for next-generation gravity missions (NGGMs) are under investigation and discussion. One of the most promising constellations are double-pairs in Bender configuration (Bender et al., 2008), i.e. two GRACE/GRACE-FO-like pairs with high-precision inter-satellite ranging, where one pair is flying in a (near-)polar orbit and the other in an inclined one, where the inclination turns out to be optimal in a range of 60° to 70°. It can be shown that with such a configuration temporal aliasing effects, which are one of the dominant error contributors of single-pair missions like GRACE and GRACE-FO and result in typical striping patterns, can be reduced significantly (in the order of a factor 5 to 10; Wiese et al., 2011, Daras and Pail, 2017). Another promising constellation is high-precision high-low tracking between high or medium orbiting and low orbiting satellites (Hauk et al., 2017), a concept which has been proposed to the European Space Agency (ESA) in response to the Earth Explorer 10 call (Pail et al., 2018).

From the instrument and payload point of view, currently the most limiting factor to a dedicated gravity field mission, especially to the retrieval of long-wavelength signals, is the performance of the accelerometer (Flechtner et al., 2016), which is required to measure the non-gravitational forces acting on the satellite. So far, in all gravity field missions, electrostatic accelerometers (EA) have been employed, offering some distinctive advantages such as an extremely high short-term sensitivity as well as robustness towards launch and space environment. However, they also suffer from certain drawbacks like (uncontrollable) thermal drift in the low frequency range below a few mHz and scale factor instabilities (Christophe et al., 2018, Klinger and Mayer-Gürr, 2016).

A new generation of instruments, relying on the manipulation of matter waves through atom interferometry, appears nowadays as very promising candidates for inertial measurements of high precision and accuracy. Cold Atom interferometers (CAI) have already proven on ground to be very high-performance sensors with the development of cold atom gravimeters (Peters et al., 2001), gravity gradiometers (McGuirk et al., 2002) and gyroscopes (Gustavson et al., 1997) in recent decades. This promising technology has demonstrated on-ground performances that compete with other state-of-the-art inertial sensors and is only expected to reach its full potential in space-based applications. In such a micro-gravity environment, the free fall time of the atoms in the instrument

and therefore, the measurement scale factor, can be increased by orders of magnitude compared to ground-based sensors.

These two types of instruments have their own assets which are, for the electrostatic sensors, their demonstrated short-term sensitivity and their proven flight heritage, and for atom interferometers, amongst others, the time-invariant measurement stability as well as the absolute nature of the measurements, thus making calibration processes obsolete. These two technologies seem in some aspects very complementary and a hybrid sensor bringing together all their assets opens new perspectives in terms of space-based inertial measurements. Following this idea, we study an instrument configuration where the EA's bias is periodically estimated through CAI measurements and then corrected with a specific gain. This gain then determines the rate at which the EA is recalibrated and is dependent on the EA and CAI performance. The hybridization is expected to be an important step towards significantly improving the quality of satellite-based gravity field retrieval. Its technological aspects as well as its impact on satellite gravimetry is subject of a currently ongoing joint ESA study between ONERA and TUM (Contract No. *RFP/3-15194/17/NL/FF/mg*).

This paper aims to evaluate and quantify the additional value of a hybrid accelerometer compared to a regular EA for the performance of satellite-based gravity field determination in the context of a GRACE-type and Bender-type mission and its corresponding requirements by means of numerical closed loop simulations which incorporate the novel instrument's specifications.

The manuscript is structured as follows. In chapter 2 the simulation environment alongside all relevant parameters is discussed. In chapter 3 the simulation results based on different signal and error contributions to the observation system are presented and analysed. Also, the influence of the scale factor uncertainty is investigated. Chapter 4 summarizes the key findings and draws conclusions towards future developments.

2 Simulation environment and parameters

The simulations presented in this study have been conducted on IAPG's closed-loop reduced-scale simulation software which is described in detail in Murböck (2015) and Murböck et al. (2014). Compared to a real gravity mission processing scheme this tool uses various simplifications as a trade-off for improved computation time. The most important aspects which are of relevance for the study are reviewed in the following.

First, externally generated Keplerian orbits and gravity field background models consisting of a static component as well as its tidal and non-tidal temporal variations – the two latter being optional – are introduced. In this study, we use repeat orbits for both satellite pairs (Tab. 1) with a total mission period of 30 days and a sampling interval of 10 s. The initial mean anomaly for each satellite is selected in such a way that the inter-satellite distance within each satellite pair amounts to approximately 200 km. For the description of the static part of the gravity field the model GOCO03s (Mayer-Gürr et al., 2012, Pail et al., 2010) is used. The updated ESA Earth System Model (Dobslaw et al., 2014) represents non-tidal temporal variations induced by mass transport processes within atmosphere (A), ocean (O), continental hydrology (H), ice (I) and solid earth (S). Finally, the tidal variations are introduced through a difference of the models FES2004 (Lyard et al., 2006) and EOT08a (Savchenko and Bosch, 2008), both containing the eight major diurnal and semi-diurnal tidal constituents Q1, O1, P1, K1, N2, M2, S2 and K2. We note that the simulation results are evaluated on the level of residuals, meaning that the focus does not lie on the output gravity field but rather on its retrieval error (difference between output and input) resulting from the sum of error sources added to the simulation environment. Due to the implementation of the reduced-scale simulator (explained

in the following) this process is linear; it is therefore irrelevant whether the temporal variations are introduced on signal level and subtracted at the end (as done for AOHIS) or whether they are directly introduced on the level of errors (as done for the ocean tides).

[placeholder for Table 1 – see attachment]

Based on this information gravitational accelerations are calculated in a next step by means of a spherical harmonic (SH) synthesis for each satellite at every epoch and are then used to generate the final observations for the simulations. Within the reduced-scale simulator they are set up in terms of line-of-sight (LOS) acceleration differences which read, according to Murböck (2015),

$$\hat{l}_{ll-SST} = \langle \Delta a_{grav}, \Delta r_{LOS} \rangle \tag{1}$$

Here, Δa_{grav} is assumed to be free of any non-gravitational components, i.e.

$$\langle \Delta a_{grav}, \Delta r_{LOS} \rangle = \langle \Delta a_{total}, \Delta r_{LOS} \rangle - \langle \Delta a_{non-grav}, \Delta r_{LOS} \rangle \tag{2}$$

In the equations above, Δ describes the difference between the satellites, Δa_{grav} the gravitational acceleration differences containing the gravitational potential gradient differences and Δr_{LOS} the LOS vector pointing from one satellite's centre of mass to the other's. This observation type serves as an approximation of the main ll-SST observable – the range between satellites resp. its variation based on time and geolocation. However, contrary to those, range accelerations pose a direct functional of the gravitational potential, thus making the adjustment problem at hand a linear one, ultimately leading to a significantly improved computational efficiency. It will be shown in section 3.1 that the results are in accordance with those of a full-fledged gravity retrieval applying the short-arc method to range-rate observations, so that the results obtained by the reduced-scale simulator can be considered as representative and conclusive.

In order to simulate realistic observation behaviour instrument accuracy needs to be taken into account. This is done by projecting the noise of each considered instrument in the simulation onto the LOS between a pair of satellites, accumulating the results into a single time series in terms of range accelerations and finally, adding it onto the error-free observations generated in the previous step. In this study, we only take into account the two most dominant instruments: the accelerometer and the laser ranging interferometer (LRI). The LRI's noise specification is taken from ESA's SC4MGV final report (Iran-Pour et al., 2015) and in terms of range accelerations reads

$$d_{range-acc.} = 2 \cdot 10^{-8} \cdot (2\pi f)^2 \cdot \sqrt{\left(\frac{10^{-2} Hz}{f}\right)^2 + 1} \frac{m}{s^2 \sqrt{Hz}} \tag{3}$$

It is shown in terms of amplitude spectral densities (ASD) as a thick dashed grey curve in Figure 1.

[placeholder for Figure 1 – see attachment]

For the accelerometer noise we use the hybrid instrument's specifications provided by ONERA. Figure 1 shows different hybridization options which deviate from each other by a different noise level of the CAI. As a reference, the error curve of a regular EA is shown (black solid curve). The scenario *case 1* corresponds to achieved on-ground performance with state-of-the-art cold atom gravimeters (Farah et al., 2014, Freier et al., 2016), but is to be regarded as rather pessimistic in the context of a space-based application. Here, *case 2* seems to be more realistic considering the current

level of CAI technology, while *case 3* is to be regarded as rather optimistic. Additionally, we simulate a kind of an ideal hybridization scenario, *case 4*, where the noise level of the CAI is able to extend the white noise behaviour of the EA in the measurement bandwidth down to very low frequencies.

Since the EA/CAI-hybridization is currently realized in just one axis, it is reasonable to use it for along-track measurements where due to atmospheric friction the majority of non-gravitational accelerations can be expected. We assume that each satellite (and hence its accelerometer) is oriented in a way where its (hybrid) X-axis is aligned with its current velocity vector which is tangential to the orbit (along-track), the Z-axis points in radial direction, and the Y-axis represents the cross-track direction normal to the plane spanned by X and Z to complete a right-handed system. Since the velocity vector and the LOS do not coincide (based on the parameters defined in Tab. 1 their deviation constitutes between 0.9° and 3.9° depending on on geolocation), observations in Y and Z which are still done with the uncalibrated EA inevitably dominate the low-frequency spectrum of the LOS projection (Fig. 2a). This does not represent the full potential of the hybridization and can be regarded as a kind of a worst-case scenario.

The advantages of the hybridization can be maximized if one assumes that both satellites of a pair are oriented along their LOS, which approximately is the case for the GRACE and GRACE Follow-On missions. Here, the Y and Z measurements have no further contribution to the LOS projection of the accelerometer noise (Fig. 2b). This is to be considered as best-case, as in reality accelerations in any spatial direction directly impact the inter-satellite ranging and thus, the gravity retrieval performance. For the simulations at hand, this scenario can be seen as an equivalent of a full three-dimensional hybridization under the assumption of the previously described satellite orientation in along-, cross- and radial direction. The results obtained by both scenarios are shown in this paper, the former being referred to as 1D- and the latter as 3D-hybridization. In order to quantify the gain in solution quality obtained through the hybrid accelerometer a reference scenario featuring a stand-alone EA instead of a hybrid instrument is also simulated.

[placeholder for Figure 2 – see attachment]

For sake of completeness we note that in addition to the LRI and the accelerometer noise attitude reconstruction errors (star camera) may also become a relevant factor in case the accelerometer performance in the low-frequency bandwidth is substantially improved. In this study it could be shown that this effect would only become notable if *case 4* is used (primarily if the 3D-hybridization is assumed) and no temporal variations of the gravity field are considered in the simulations.

The observation weighting is done by means of a cascade of digital Butterworth ARMA filters (Siemes 2008, Pail et al., 2011). The filter coefficients are chosen in such a way that the cascade's frequency response optimally matches the inverse of the amplitude spectrum of the previously generated instrument noise time series. In the reduced-scale simulator the co-variance resp. the weighting matrix is never explicitly set up at any point. Instead, the filters are consecutively applied to each column of the design matrix and the right-hand side. This approach may suffer from filter warm-up effects, which can be counteracted by excluding a number of starting observations (e.g. 1000) from entering the estimation process. This approach has no significant negative impact on the final gravity field solution as long as the number of the remaining observations significantly exceeds that of the omitted ones. Otherwise, methods for reconstruction of the omitted information could be employed (Siemes, 2008).

In a last step – the spherical harmonic analysis – the previously generated normal equation system can be inverted and solved based on a regular Gauss-Markov least squares scheme producing an output gravity field model in terms of spherical harmonic coefficients. One can then subtract the

input models from the result in order to evaluate the retrieval errors. In case of the AOHIS model its mean value over the retrieval period must be considered, while the ocean tide model is not subtracted as it is already introduced in terms of residuals. It should be noted that in closed-loop simulations where the instruments constitute the only source of observation noise, SH coefficient residuals have approximately equal amplitudes as their formal errors. Because the latter precisely depict the instruments' effect on the gravity field retrieval and due to their homogenous nature, it may be reasonable to base the evaluation of the results of such simulation scenarios on formal errors instead of the coefficients in this specifc case.

Due to several simplifications of reduced-scale simulations their results should be validated against full-fledged simulation results. This can be accomplished by a comparison to IAPG's full-scale simulation tool (Daras, 2016, Daras and Pail, 2017), where all relevant aspects of a real gravity field mission simulation and the subsequent gravity retrieval can be taken into account. The software is based on the short-arc approach (Schneider, 1969) with built-in numerical orbit integration. In contrast to the reduced-scale simulator, the stochastic model is not introduced via ARMA filtering, but an error auto-covariance matrix for each arc. Thus, the arcs are considered as uncorrelated, with the exception of boundary conditions applied to avoid jumps of the reference orbit at the transition of successive arcs. While for the majority of applications the full-scale simulator can be expected to yield the most reliable results, it is not optimally suited for this study. Depending on arc length it is possible that information concerning the long wavelengths of the spherical harmonic spectrum of the gravity field (periods longer than the chosen length of the short arc) where we expect the highest impact of the hybrid accelerometer cannot be handled adequately due to the artificial decorrelation of individual arcs. Theoretically, this issue can be remedied by increasing the arc length; however, it was shown that as a consequence of the current implementation of the full-scale simulator a greater arc length in combination with large variations in instrument noise amplitudes can lead to numerical instabilities due to the long-wavelength characteristics of the weighting matrix.

3 Numerical Simulations and Results

In this chapter the impact of the hybrid instrument on the performance of gravity field retrieval is assessed and quantified based on a number of numerical closed-loop simulations. In a first group of experiments, we disregard temporal gravity signals and thus also temporal aliasing errors, and only take instrument errors of the accelerometer and the LRI into account. Afterwards, we include also temporal gravity to compare the error contribution related to temporal aliasing with the instrument errors. At the end of this chapter, we address another important aspect that is related to a systematic error component induced by the accelerometer: the fact that the accelerometer scale factor cannot be determined perfectly, resulting in an imperfect scaling of the accelerometer measurements over the complete frequency bandwidth. One of the advantages of the hybrid accelerometer compared to an EA is that the scale factor can be determined more accurately.

3.1 Instruments only

We first conduct simulations taking into account only the observation errors induced by the accelerometer and the LRI according to Fig. 1. Figure 3 shows the results for these different scenarios in terms of degree RMS of the difference between the input and output model (c.f. chapter 2) for a GRACE-type mission scenario according to

$$c_{n,RMS} = \sqrt{\sum_{m=0}^{n} \left(\left(\bar{C}_{nm,out} - \bar{C}_{nm,in} \right)^2 + \left(\bar{S}_{nm,out} - \bar{S}_{nm,in} \right)^2 \right)} \quad (4)$$

where n and m are the SH degree resp. order and $\bar{C}_{nm}$ and $\bar{S}_{nm}$ are the fully normalized SH coefficients of the input resp. output model. Equivalently, the formal errors according to

$$\sigma_{c_{n,RMS}} = \sqrt{\sum_{m=0}^{n} \left(\sigma^2_{\bar{C}_{nm,out}} + \sigma^2_{\bar{S}_{nm,out}} \right)} \quad (5)$$

are shown. As expected, the impact of the hybrid accelerometer measurements compared to the EA is mainly reflected in, but not limited to, the long-wavelength part of the gravity field solution. It is also evident that not all hybridization scenarios lead to an improvement of the solution quality compared to a standard EA. As can be seen in Fig. 3 no significant differences can be detected between the coefficient residuals of the reference EA scenario and those of *case 1* and *2*. This is further underlined in Table 2, which shows the RMS of global height anomaly differences calculated from the residual coefficients. This behaviour can be attributed to the fact that the accelerometer improvement obtained by *case 1* lies below the frequency bandwidth that is relevant for gravity field retrieval. The lower boundary of this frequency band is defined by the satellites' orbital frequency which is approximately $1.8 \cdot 10^{-4}$ Hz (equivalent to one complete revolution in about 90 minutes) for both the polar and the inclined pair. In *case 2* the recalibration of the EA occurs at a frequency that is very close to the edge of the retrieval band. Therefore, no significant difference to the reference scenario can be found here either. Due to the same reason the results of these two scenarios do not differ between 1D- and 3D-hybridization (cf. Fig. 3). First significant improvements with respect to the standard scenario become apparent when using *case 3*. Here, the degree RMS of the residuals improve by up to a factor 3 in the SH degrees below *n*=10 in case of a 3D- and marginally less in case of a 1D-hybridization. *Case 4* offers the most substantial gain in performance: The flat noise spectrum in the 3D-scenario can be attributed for an improvement of up to over one order of magnitude in the spectrum below *n*=10. Compared to 3D, the assumption of a one-dimensional hybridization leads to an overall decrease in performance in the low to medium degrees. Nevertheless, the improvement with respect to the reference scenario is still substantial.

[placeholder for Figure 3 – see attachment]

It is notable that specifically for *case 3* and *4* the gain in retrieval performance is not limited to the frequency bands specified in Fig. 1, but instead extends into higher degrees of the spectrum. To a lesser extent, a similar behaviour can be seen for *case 2*. The impact of hybridization can also be quantified in further detail by analysing the respective formal error triangles of the different cases. Figure 4 shows the relative improvement of the formal errors of *case 3* and *case 4* with respect to the reference EA scenario. While improvements made in a certain frequency band are almost linearly propagated into the corresponding (near-)zonal coefficients (cf. Fig. 1), they may significantly influence higher-degree sectorial as well as tesseral coefficients of higher orders. This is due to the fact that there is no one-to-one relation between the instrument's frequency spectrum (related to time domain of the orbit track) and the spherical harmonic spectrum (related to the space domain of the sphere) (Rummel et al. 1993, Pail, 2017). Mathematically, it can be shown that sectorial coefficients of a certain degree contain more low-frequency information than zonal coefficients of

the same degree. Inversely, while the influence of an improved long-wavelength behaviour of the accelerometer is limited to rather low degrees for (near-)zonal coefficients, much higher degrees of (near-)sectorial coefficients are influenced. Physically, this behaviour can be explained by the fact that the along-track inter-satellite ranging measures close to North-South direction and therefore has the highest sensitivity for (near-)zonal coefficients, while the East-West direction (reflected by (near-)sectorial coefficients) can be observed much worse. Beside temporal aliasing effects, this anisotropic error structure is the second main reason for the typical GRACE striping pattern. Consequently, a better decorrelation of the observation errors, which is in our case achieved by a reduction of along-track long-wavelength accelerometer errors, has a relatively high impact on (near-)sectorial parameter groups.

[placeholder for Figure 4 – see attachment]

For a Bender-type mission the overall level of the coefficient residuals is significantly lower than for a GRACE-type one as can be seen in Fig. 5. This can mainly be attributed to the improved observation geometry which, amongst others, now allows for the registration of East-West-components of the gravity field. Therefore, the accelerometer stability plays a much smaller role towards the solution quality than in case of a single-pair mission. Compared to the latter, *case 3* shows only marginal improvements with respect to the standard scenario which are now limited to SH degrees n<5. The performance gain granted by *case 4* is now also limited to degrees below n=20. Nevertheless, it allows for improvements of up to one order of magnitude in the very low degrees up to n=5 which is still substantial with regard to time-variable gravity applications. The differences between 1D- and 3D-hybridization are basically non-existent for *case 1* to *3* and can only be made out to some extent in the solutions of *case 4*, where a gain in performance of a factor of 3 at the very low degrees – gradually decreasing towards n=10 – can be seen.

[placeholder for Figure 5 – see attachment]

The results presented above are now validated by those obtained through full-scale simulations. Due to the problems concerning proper observation weighting in the full-scale simulator (cf. chapter 2) only simulation scenarios for *case 2* to *4* under assumption of a 3D-hybridization could be properly computed. The full-scale results shown in Fig. 6 seem to exhibit a highly consistent behaviour with the reduced-scale ones depicted in Fig. 3 and 5. While the total amplitudes of the residuals and the rate at which the retrieval error increases with respect to SH degree differ slightly between full- and reduced scale, the relative behaviour among the solutions is very similar. These differences can be attributed to the different processing strategies as described in chapter 2. Based on these validation results, the results obtained through reduced-scale simulations can be considered as reliable.

[placeholder for Figure 6 – see attachment]

3.2 Instruments and temporal signal

Adding temporal variations to the simulation system induces temporal aliasing which degrades the gravity retrieval performance. At first, we include only non-tidal HIS signals, thus optimistically assuming the atmosphere and ocean (AO) signals, which due to their rather short

periods contribute the most to temporal aliasing errors, can be perfectly reduced by a priori de-aliasing strategies.

Figure 7 shows that the introduction of the HIS component to the observations leads to a significant decrease in solution quality, as the temporal HIS aliasing superimposes instrument (mainly accelerometer) errors. Therefore, only the results of 3D-hybridization simulations are shown. Some improvements can be found in the solutions of *case 3* and *4* below *n*=10 for the GRACE-type mission. From there onwards, variations between the respective difference degree RMS – constituting a factor 3 at maximum – can be distinguished up to about *n*=45, although the overall level of the difference degree RMS remains practically the same. Nevertheless, this behaviour suggests that the improved performance of the accelerometer may still have an influence on this part of the spectrum. As already for the previously shown instrument-only simulations, the overall retrieval error for a Bender-type mission is significantly lower than for a GRACE-type mission. While some gains due to an improved accelerometer can be seen for *case 3* and *4* – *case 4* once again showing the best performance – they are mostly limited to degrees below *n*=5 and are in direct comparison to a single-pair mission far less distinctive. From *n*=5 upwards, none of the scenarios show any significant variations with respect to each other which indicates that for a double-pair mission the accelerometer does not impact the gravity field retrieval except for the very long-wavelength part of its spectrum. This behaviour can also be clearly seen in the global height anomaly error RMS in Table 2: While *case 4* shows an improvement of around 20% with respect to *case 1* at *n*=5, it already decreases to below 5% at *n*=20.

[placeholder for Figure 7 – see attachment]

[placeholder for Figure 8 – see attachment]

[placeholder for Figure 9 – see attachment]

Adding the full non-tidal temporal signal (AOHIS) to the simulation environment once again increases the aliasing effects due to the short periods and at the same time high amplitudes of the AO-component, limiting the retrieval performance even further (Fig. 8). It is noted that this should be considered as an unrealistic worst-case scenario when not applying any AO de-aliasing strategies. While in case of HIS some notable differences between the simulations scenarios could be found for a GRACE-type mission, only marginal discrepancies well below a factor of 2 can be seen in the low degrees in case of AOHIS. For a double-pair mission practically no gains at all are to be found in the entire gravity field spectrum.

Additionally including the ocean tides into the simulations further decreases the gravity solution's sensitivity towards the improved accelerometer performance (Fig. 9). The retrieval error now does not depend on the accelerometer error level of each hybridization scenario due to the very high level of the temporal aliasing effects induced by the high-frequency tide signal. This holds for both a GRACE-type and a Bender-type mission.

The results presented above clearly illustrate that a solution based on a double-pair mission is at best barely influenced by the accelerometer's behaviour if temporal variations are included in the simulations. However, it is reasonable to assume that a reduction of the temporal aliasing to a sufficiently low level may amplify the accelerometer's impact. We therefore apply the Wiese parametrization (Wiese et al., 2011; Daras and Pail, 2017) where low-resolution gravity fields for shorter time periods are estimated alongside the full solution, ultimately leading to an improvement of the latter. For this study, the best results could be obtained by co-estimating daily gravity fields up to degree and order 15. It should be noted that, according to the Nyquist theorem, this choice of

parameters mainly contributes towards the de-aliasing of the AO part, as the highly correlated A- and O-components' periods average at around two days. On the other hand, no gain is to be expected for the reduction of the aliasing induced by tidal signals. In contrast to non-tidal signals, they are related to well-defined (mainly semi-diurnal and diurnal) excitation frequencies and are mapped to much longer aliasing periods along the satellite orbit. The gain of an additional daily parameterization is therefore very limited. Instead, they should rather be co-estimated by dedicated tidal parameterization (Hauk and Pail 2018).

While the Wiese parametrization indeed leads to an overall decrease of temporal aliasing, the impact of the accelerometer does not become more prominent within the full gravity solutions than without this de-aliasing approach. However, its impact can now be seen to some extent in the co-estimated daily fields. In Fig. 10 the mean of the daily solutions as well as of daily variations are depicted, the latter being calculated from differences between every two consecutive days. The results suggest that while the daily solutions resp. variations cannot be resolved to a higher SH degree, they can nevertheless be retrieved with a higher accuracy when using the *case 4* hybridization scenario. In case of both HIS and AOHIS, it allows for an increase in retrieval performance of daily variations by around a factor 2 in terms of degree RMS of residuals towards the regular EA. This poses an important aspect with regard to NGGM requirements.

[placeholder for Figure 10 – see attachment]

[placeholder for Table 2 – see attachment]

3.3 scale factor study

Finally, we investigate the impact of the accelerometer scale factor. Per definition, the scale factor describes the ratio between an instrument's input and output signal. For this study, we assume a gravity field mission flying in drag free mode as specified in many NGGM requirements. Therefore, only the (non-compensated) residual non-conservative accelerations (dominated by drag) are measured by accelerometer. This so-called residual drag is the part of the non-gravitational signal that can be detected by the accelerometer but not corrected by the satellite's impulse thrusters due to their inability to generate a sufficiently small counter-thrust. Instead, this signal fraction is reduced from the observations during the data processing. By applying the scale factor to the residual drag we effectively describe its improper reduction conditioned by erroneous measurements. We then add the result to the total noise time series. Comparing the ASDs of the total noise with and without the addition of the scaled residual drag allows for a first insight into whether the scale factor uncertainty significantly contributes to the total retrieval error.

The specifications of the residual drag are taken from ESA's SC4MGV final report and are visualized in Fig. 11a. The scale factor is defined by ONERA as 10^{-5} for the calibrated (hybrid) axis due to the absolute nature of its measurements and as 10^{-2} for the uncalibrated (regular EA) ones. It is further assumed that the scale factor remains constant over the complete observation period.

[placeholder for Figure 11 – see attachment]

Fig. 11b shows that in case of a regular EA the scale factor negatively influences the overall noise level in the spectrum above 1 mHz. Here, a noise increase of 100% can be asserted. For the simulations at hand, however, it only plays a pronounced role over a small spectral range up to around 2-3 mHz where the LRI noise then becomes the dominant error component. In order to

quantify the scale factor's impact on the retrieval error an additional simulation which uses a new stochastic model generated on the basis of the new total noise time series (cf. section 2) is carried out. We note that the scale factor is hereby implicitly treated as a stochastic effect. As can be deduced from Fig. 11d the small noise increase induced by the scale factor distinctly degrades the solution quality – the respective formal errors reveal a decrease in retrieval quality by a factor 2 above SH degree n=10 for a GRACE-type mission and even earlier for a Bender-type mission. This behaviour is explained in detail in section 3.1. We note that these scale factor simulations are only presented for a scenario where the temporal variations of the gravity field are excluded, as the hereby induced temporal aliasing errors widely superpose the effect of the scale factor.

If the observations are now assumed to be based on hybrid measurements, the scale factor uncertainty becomes widely negligible for the overall solution quality (cf. Fig. 11c). It is irrelevant whether the hybridization is realized in one axis (the only precondition being that the hybridization is implemented in along-track) or all three.

4 Summary and Conclusions

In this paper we investigate the impact of a novel hybrid accelerometer consisting of a standard electrostatic component and a cold atom interferometer on the performance of gravity field retrieval in the context of a GRACE- and Bender-type satellite formation. This is done by means of numerical closed-loop simulations where four different accelerometer noise specifications are considered and different components of the total gravity field signal (static, non-tidal and tidal temporal variations) are gradually added to the observation system. We also distinguish between a 1D- and a 3D-hybridization, the former assuming hybrid measurements in along-track direction only, and the latter additionally in cross-track and radial directions.

In an instrument-error-only simulation scenario the results indicate that retrieval performance depends primarily on the accuracy level that can be reached with the CAI and thus, the recalibration rate of the EA. If the recalibration (crossing point between the error curves of the CAI and the EA) happens below the orbital frequency (*case 1*) no gain in retrieval performance is achieved in comparison to a standard EA. Vice versa, if the CAI reaches a comparable error level as the EA in its designated measurement bandwidth, i.e. a flat noise spectrum is realized (*case 4*), the improvement is maximal with up to 80% in terms of global height anomaly difference RMS. It is also shown that improvements made at low frequencies propagate into high-degree sectorial and high-degree and order tesseral spherical harmonics. As an example, for *case 3* a gravity retrieval gain of a factor of 2 compared to a pure EA can be reached for (near-)sectorial coefficients around SH degree n=30, a further improved noise level of the CAI by one order of magnitude, as it is realized in *case 4*, leads to the same improvement of (near-)sectorial coefficients around degree 80 to 90.

The results presented in this paper also clearly demonstrate that the relative impact of the accelerometer measurements decreases if the overall observation geometry is improved, e.g. by adding an inclined second satellite pair in Bender configuration. While an overall performance improvement of up to 30% (in terms of global height anomaly difference RMS) can be achieved by the optimistic hybridization scenario (*case 3*) even at degree n=50 for GRACE-type mission, the same hybridization scenario yields only a gain of 20% for a Bender-type formation at n=5. Still, a distinctive gain in retrieval performance can be yielded for a double-pair mission by assuming a flat accelerometer noise spectrum up to SH degree n=20 (75% in terms of global height anomaly error RMS). The reduced-scale results are validated by selected full-scale simulations with equal simulation parameters, revealing a high consistency in a relative as well as in an absolute sense.

Adding temporal variations of the gravity field to the simulation environment widely camouflages any gains obtained by the hybrid accelerometer. While in case of HIS aliasing some variations between the hybridization scenarios can be detected for a GRACE-type mission and even, to a far lesser extent, for a Bender-type one, they become marginal in case of additional AO and ocean tide aliasing. Regarding non-tidal (especially AO-induced) aliasing, for a Bender-type mission the reduction of temporal aliasing can be attempted by parametrizing daily signals (Wiese approach). While the results of all four accelerometer scenarios still cannot be distinguished in the full 30-days solution, at least the gain of *case 4* can now clearly be seen in the daily fields, and most importantly, their variations obtained by this processing strategy. For HIS, the daily variations can be retrieved with up to a 25% higher accuracy (in terms of global height anomaly error RMS) in comparison to the standard EA, while for AOHIS the gain is at approximately 30%.

Finally, the accelerometer's scale factor uncertainty is investigated, where we implicitly assume the satellites to be flying in drag-free mode. It is shown that in a standard EA scenario a degradation of up to 15% in terms of global height anomaly difference RMS can be observed when including a 10^{-2} scale factor uncertainty in the simulation. In contrast, in the hybrid case it can be assumed that the scale factor can be determined down to 10^{-5}. Numerical simulation results show that this small remaining uncertainty has effectively no impact on the total retrieval performance, provided that at least the along-track observations are done by a hybrid axis.

The results presented in this paper prove that even under consideration of the most pessimistic hybridization scenario the retrieval performance is at worst equal to one where a stand-alone EA is used. With an implementation of the optimistic hybridization scenario, the performance of the EA can be surpassed in a GRACE-type scenario and less distinctly in a Bender-type one. Contrary to the EA, however, the hybrid instrument with its current overall noise specifications also seems to be widely independent of scale factor uncertainties. The main aspect advocating the implementation of a hybrid accelerometer, especially with regard towards the conditions set for a NGGM, is that a flat accelerometer noise spectrum can ultimately be achieved, thus fully compensating the main drawback of a stand-alone EA. Hereby, the retrieval of the long-wavelength spectrum of the gravity field, which is of high interest for global mass variation studies, can be greatly improved. This advantage of the "perfect" hybridization is clearly underlined by the results in this paper, thus setting its realization an important future goal. In order to maximize its potential, the application of de-aliasing techniques, especially for non-tidal AO signals and the tidal component of the gravity field, shall be a decisive factor. This is a reasonable demand for the upcoming decades, as first results by Daras and Pail (2017) as well as Hauk and Pail (2018) have shown. The results of this study clearly encourage to further improve, in parallel to the processing strategies, also the performance of the key instruments, particularly the accelerometers.

Acknowledgements

A big part of the investigations presented in this paper was performed in the framework of the study "Hybrid Atom Electrostatic System Follow-On for Satellite Geodesy", ESA-ESTEC, Contract No. *RFP/3-15194/17/NL/FF/mg* funded by the European Space Agency.

References

Bender, P.L., Wiese, D.N. and Nerem R.S. (2008). A possible dual-grace mission with 90 degree and 63 degree inclination orbits. In: Proceedings, 3rd International Symposium on Formation Flying, Missions and Technologies. ESA/ESTEC, Noordwijk, pp 1–6.

Christophe, B., Foulon, B., Liorzou, F., Lebat, V., Boulanger, D., Huynh, P.-A., Zahzam, N., Bidel, Y., Bresson, A. (2018). Status of Development of the Future Accelerometers for Next Generation Gravity Missions. In: International Association of Geodesy Symposia. Springer, Berlin, Heidelberg, doi: 10.1007/1345_2018_42

Daras, I. (2016). Gravity Field Processing Towards Future LL-SST Satellite Missions; Deutsche Geodätische Kommission der Bayerischen Akademie der Wissenschaften, Reihe C, Dissertationen, Heft 770, Verlag der Bayerischen Akademie der Wissenschaften, ISBN(Print) 978-3-7696-5182-9, ISSN 0065-5325, 2016.

Daras, I. and Pail, R. (2017). Treatment of temporal aliasing effects in the context of next generation satellite gravimetry missions. Journal of Geophysical Research: Solid Earth, 122(9):7343-7362, doi: 10.1002/2017JB014250

Dobslaw, H., Bergmann-Wolf, I., Dill, R., Forootan, E., Klemann, V., Kusche, J. and Sasgen, I. (2014). The Updated ESA Earth System Model for Gravity Mission Simulation Studies. Journal of Geodesy, 89(5): 505-513, Springer Berlin Heidelberg, doi: 10.1007/s00190-014-0787-8

Drinkwater, M.R., Floberghagen, R., Haagmans, R., Muzi, D. and Popescu, A. (2003). GOCE: ESA's first Earth Explorer Core mission. In: Beutler, G., Drinkwater, M.R., Rummel, R., von Steiger, R. (eds.), Earth Gravity Field from Space – From Sensors to Earth Sciences, Space Sciences Series of ISSI, vol. 17. Springer, Dordrecht, The Netherlands, S. 419–432, ISBN (print): 1-4020-1408-2, doi: 10.1007/978-94-017-1333-7_36

Farah, T., Guerlin, C., Landragin, A., Bouyer, P., Gaffet, S., Pereira Dos Santos, F. and Merlet, S. (2014). Underground operation at best sensitivity of the mobile LNE-SYRTE Cold Atom Gravimeter. Gyroscopy and Navigation, 5(4): 266-274, doi: 10.1134/S2075108714040051

Flechtner, F., Neumayer, K.H., Dahle, C., Dobslaw, H., Güntner, A., Raimondo, J.C. and Fagiolini, E. (2016). What can be expected from the GRACE-FO Laser Ranging Interferometer for Earth Science applications? Surveys in Geophysics, 37(2): 453-470, doi: 10.1007/s10712-015-9338-y

Flechtner, F., Dahle, C., Landerer, F., Webb, F., Watkins, M., Massmann, H. and Bettadpur, S. (2018). GRACE Follow-On: Current Mission Status and next steps. Geophysical Research Abstracts, vol. 20, EGU2018-8990

Freier, C., Hauth, M., Schkolnik, V., Leykauf, B., Schilling, M., Wziontek, H., Scherneck, H.G., Müller, J. and Peters, A. (2016). Mobile quantum gravity sensor with unprecedented stability. Journal of Physics: Conference Series 723, 012050, doi:10.1088/1742-6596/723/1/012050

Gustavson, T.L., Bouyer, P. and Kasevich, M.A. (1997). Precision Rotation Measurements with an Atom Interferometer Gyroscope. Physical Review Letters, 78: 2046-2049, doi:10.1103/PhysRevLett.78.2046

Hauk, M., Schlicht, A., Pail, R.and Murböck, M. (2017). Gravity field recovery in the framework of a Geodesy and Time Reference in Space (GETRIS). Advances in Space Research, 59(8): 2032-2047. doi: 10.1016/j.asr.2017.01.028

Hauk, M. and Pail, R. (2018). Treatment of Ocean Tide Aliasing in the context of a Next Generation Gravity Field Mission. Geophysical Journal International, 214(1): 345–365, doi: 10.1093/gji/ggy145

Iran Pour, S., Sneeuw, N., Daras, I., Pail, R., Murböck, M., Gruber, T., Tonetti, S., Cornara, S., Weigelt, M., Van Dam, T., Visser, P. and Teixeira da Encarnação, J. (2015). Assessment of satellite constellations for monitoring the variations in earth gravity field. SC4MGV, ESA/ESTEC Contract No. AO/1-7317/12/NL/AF, Final Report.
International Union of Geodesy and Geophysics (IUGG) (2016): IUGG Resolutions at the XXVI General Assembly 2015. In: Drewes, H., Kuglitsch, F., Adám, J., Rózsa, S. (eds.), The Geodesist's Handbook. Journal of Geodesy, 90(10): 977-980, doi: 10.1007/s00190-016-0948-z

Klinger, B., Mayer-Gürr, T. (2016): The role of accelerometer data calibration within GRACE gravity field recovery: Results from ITSG-Grace2016. Advances in Space Research, 58(9): 1597-1609, doi: 10.1016/j.asr.2016.08.007

Lyard, F., Lefevre, F., Letellier, T. and Francis, O. (2006). Modelling the global ocean tides: modern insights from FES2004. Ocean Dynamics 56(5-6): 394-415, Springer-Verlag, doi: 10.1007/s10236-006-0086-x

Mayer-Gürr, T., Rieser, D., Höck, E., Brockmann, J.M., Schuh, W.D., Krasbutter, I., Kusche, J., Maier, A., Krauss, S., Hausleitner, W., Baur, O., Jäggi, A., Meyer, U., Prange, L., Pail, R., Fecher, T. and Gruber, T. (2012). The new combined satellite only model GOCO03s, GGHS2012, Venice, Italy

McGuirk J.M., Foster G.T., Fixler J.B., Snadden M.J. and Kasevich M.A. (2002). Sensitive absolute-gravity gradiometry using atom interferometry. Physical Review A, 65: 033608, doi: 10.1103/PhysRevA.65.033608

Murböck, M., Pail, R., Daras, I. and Gruber T. (2014). Optimal orbits for temporal gravity recovery regarding temporal aliasing. Journal of Geodesy, 88(2): 113-126, doi: 10.1007/s00190-013-0671-y.

Murböck, M. (2015): Virtual Constellations of Next Generation Gravity Missions. Deutsche Geodätische Kommission der Bayerischen Akademie der Wissenschaften, Reihe C, Dissertationen, Heft 750, Verlag der Bayerischen Akademie der Wissenschaften, ISBN(Print) 978-3-7696-5162-1, ISSN 0065-5325, 2016.

Pail, R., Goiginger, H., Schuh, W.D., Höck, E., Brockmann, J.M., Fecher, T., Gruber, T., Mayer-Gürr, T., Kusche, J., Jäggi, A. and Rieser, D. (2010). Combined satellite gravity field model GOCO01S derived from GOCE and GRACE. Geophysical Research Letters, 37(20): L20314, doi: 10.1029/2010gl044906

Pail, R., Bruinsma, S., Migliaccio, F., Förste, C., Goiginger, H., Schuh, W.D., Höck, E., Reguzzoni, M., Brockmann, J.M., Abrikosov, O., Veicherts, M., Fecher, T., Mayrhofer, R., Krasbutter, I., Sansò, F. and Tscherning, C.C. (2011). First GOCE gravity field models derived by three different approaches. Journal of Geodesy 85(11): 819-843, doi:10.1007/s00190-011-0467-x

Pail, R., Bingham, R., Braitenberg, C., Dobslaw, H., Eicker, A., Güntner, A., Horwath, M., Ivins, E., Longuevergne, L., Panet, I. and Wouters, B. (2015). Science and User Needs for Observing Global Mass Transport to Understand Global Change and to Benefit Society. Surveys in Geophysics, 36(6): 743-772, Springer Netherlands, doi: 10.1007/s10712-015-9348-9

Pail, R. (2017). Globale Schwerefeldmodellierung am Beispiel von GOCE. In: Rummel, Reiner (Hrsg.): Erdmessung und Satellitengeodäsie: Handbuch der Geodäsie, herausgegeben von Willi Freeden und Reiner Rummel. Springer Berlin Heidelberg, 217-257, doi: 10.1007/978-3-662-47100-5_8 (in German)

Pail, R. and the European gravity science team (2018). Mass variation observing system by high-low inter-satellite links (MOBILE) – a mission proposal for ESA Earth Explorer 10. Geophysical Research Abstracts, vol. 20, EGU2018-1972

Peters, A., Chung, K.Y and Chu, S. (2001). High-precision gravity measurements using atom interferometry. Metrologia, 38(1): 25, doi: 10.1088/0026-1394/38/1/4

Rummel, R., van Gelderen, M., Koop, R., Schrama, E., Sansó, F., Brovelli, M., Miggliaccio, F. and Sacerdote F. (1993). Spherical harmonic analysis of satellite gradiometry. Publications on Geodesy, 39, Neth. Geod. Comm., Delft, The Netherlands.

Savcenko, R. and Bosch, W. (2008). EOT08a - Empirical Ocean Tide Model from Multi-Mission Satellite Altimetry. DGFI Report, München, Germany, 81.

Schneider, M. (1969). Outline of a general orbit determination method, in Space Research IX, Proceedings of Open Meetings of Working Groups (OMWG) on Physical Sciences of the 11th Plenary Meeting of the Committee on Space Research (COSPAR), Tokyo, edited by K. S. W. Champion, P. A. Smith, and R. L. Smith-Rose, pp. 37–40, North-Holland Publishing Company, Mitteilungen aus dem Institut für Astronomische und Physikalische Geodäsie, Nr. 51.

Siemes, C. (2008): Digital Filtering Algorithms for Decorrelation within Large Least Square Problems. Bonn: Rheinische Friedrich-Wilhelms-Universität, Hohe Landwirtschaftliche Fakultät, Dissertation

Tapley, B., Bettadpur, S., Watkins, M. and Reigber, C. (2004). The gravity recovery and climate experiment: Mission overview and early results. Geophysical Research Letters, 31(9): L09607, doi: 10.1029/2004GL019920.

Wiese, D.N., Visser, P.N.A.M. and Nerem, R.S. (2011). Estimating low resolution gravity fields at short time intervals to reduce temporal aliasing errors. Advances in Space Research, 48(6): 1094–1107, doi: 10.1016/j.asr.2011.05.027.

Attachment – Tables and Figures

Table 1
Orbit parameters

	Altitude [km]	Inclination [°]	Revolutions per nodal day	Ascending node [°]	Mean anomaly difference [°]
GRACE/Bender 1A	467	89	412/27	0	-
GRACE/Bender 1B	467	89	412/27	0	1.674
Bender 2A	461	70	167/11	0	-
Bender 2B	461	70	167/11	0	1.675

Table 2
Global height anomaly difference RMS (weighted with cosine of latitude) in [mm] for different simulation scenarios calculated up to degree 5, 20 and 50. 3D-hybridization is assumed for the hybrid accelerometer scenarios. The scenario where only the static part of the gravity field is considered is equivalent to the "instruments only" simulations

		GRACE-type			Bender-type		
Gravity signal contribution	Accelerometer scenario	n_{max}=5	n_{max}=20	n_{max}=50	n_{max}=5	n_{max}=20	n_{max}=50
static	EA	0.0056	0.0114	0.0205	0.0014	0.0015	0.0024
	case 1	0.0056	0.0114	0.0205	0.0014	0.0015	0.0024
	case 2	0.0055	0.0112	0.0203	0.0014	0.0015	0.0024
	case 3	0.0027	0.0057	0.0144	0.0011	0.0012	0.0022
	case 4	0.0004	0.0009	0.0040	0.0002	0.0004	0.0019
Static HIS	EA	0.0055	0.0253	0.0780	0.0024	0.0077	0.0149
	case 1	0.0092	0.0254	0.0759	0.0031	0.0080	0.0152
	case 2	0.0085	0.0249	0.0758	0.0038	0.0083	0.0152
	case 3	0.0054	0.0229	0.0759	0.0027	0.0078	0.0151
	case 4	0.0053	0.0217	0.0742	0.0024	0.0077	0.0150
Static AOHIS	EA	0.0462	0.1767	0.5987	0.0337	0.0770	0.1144
	case 1	0.0468	0.1737	0.5954	0.0341	0.0771	0.1145
	case 2	0.0463	0.1730	0.5956	0.0341	0.0771	0.1145
	case 3	0.0461	0.1741	0.5961	0.0339	0.0770	0.1144
	case 4	0.0460	0.1732	0.5959	0.0339	0.0770	0.1144
Static AOHIS ocean tides	EA	0.2767	0.3721	0.7199	0.0732	0.1126	0.1437
	case 1	0.2772	0.3717	0.7189	0.0738	0.1128	0.1440
	case 2	0.2769	0.3717	0.7192	0.0738	0.1129	0.1440
	case 3	0.2770	0.3723	0.7200	0.0739	0.1130	0.1441
	case 4	0.2768	0.3716	0.7193	0.0733	0.1126	0.1438

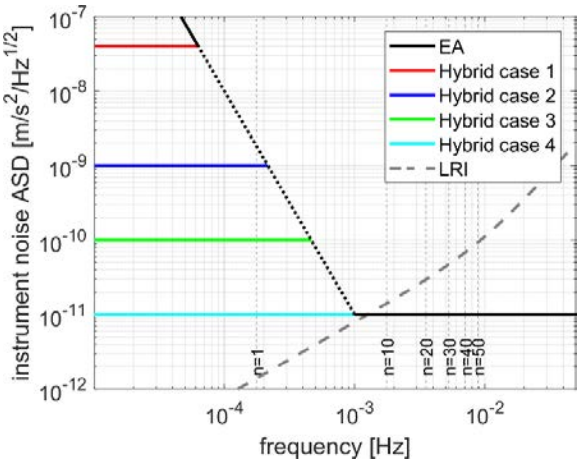

Figure 1. ASD of investigated EA/CAI hybridization scenarios and a regular EA. The dotted black line depicts the spectrum common to the respective hybrid scenario and the stand-alone EA. The thick dashed grey line represents the Laser Ranging Interferometer noise in terms of range accelerations. Vertical dashed grey lines represent the maximal contributing observation frequency to spherical harmonic coefficients of the given degree.

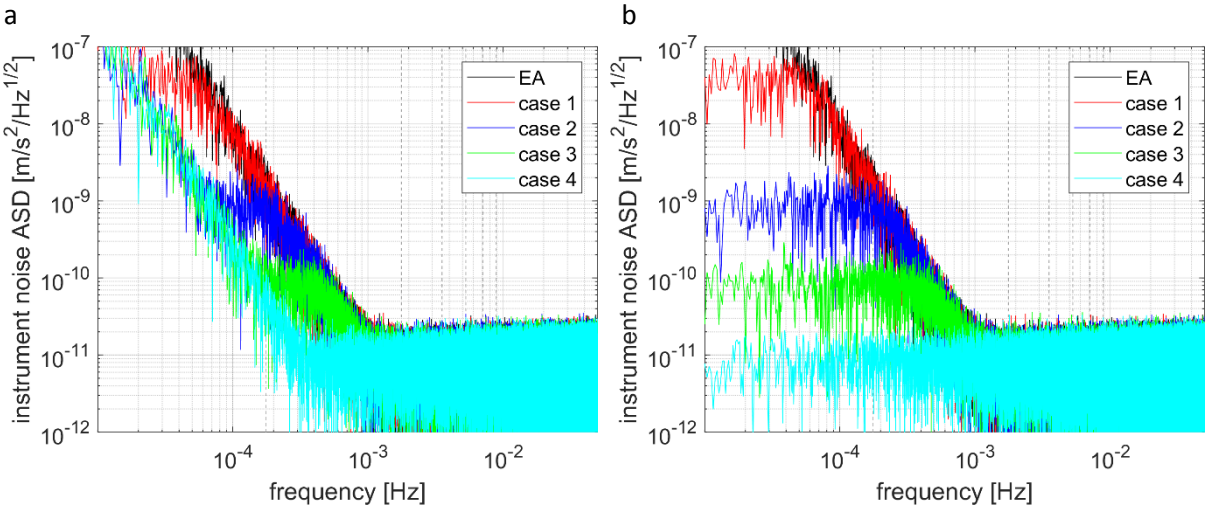

Figure 2. ASD of the LOS projection of the total accelerometer noise assuming a 1D- (a) and a 3D-hybridization (b).

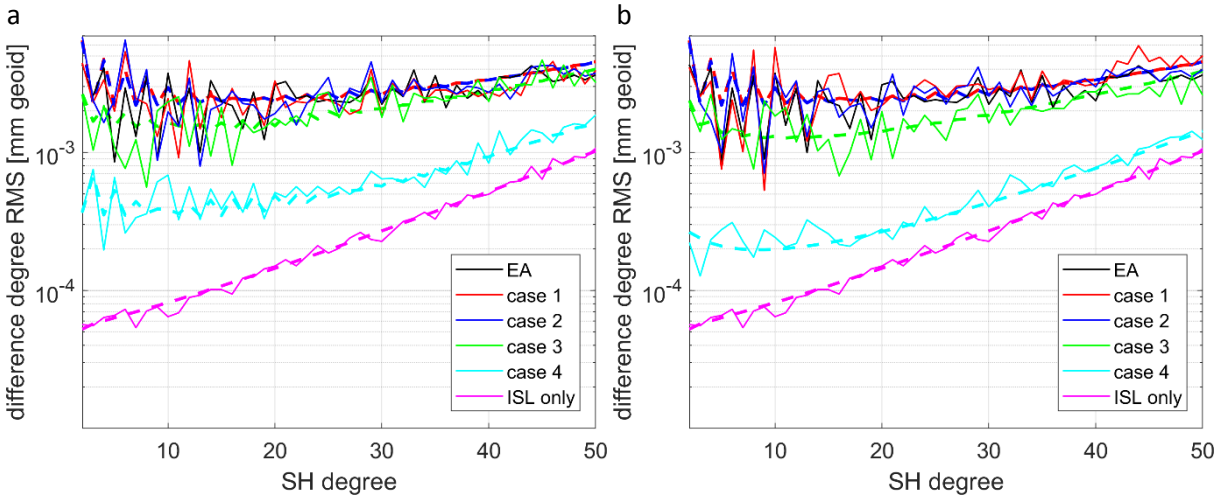

Figure 3. Degree RMS of residual coefficients for a GRACE-type mission under consideration of the static gravity field signal and instrument errors assuming a 1D- (a) and a 3D-hybridization (b). The respective formal errors are shown as dashed lines of the corresponding colour.

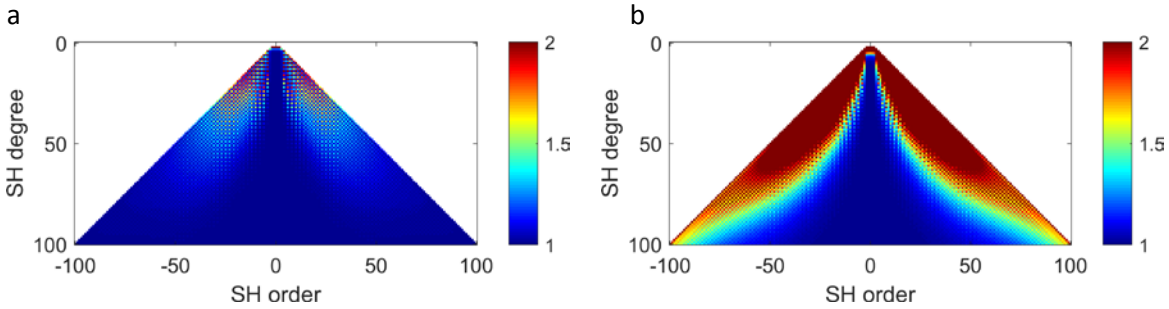

Figure 4. Relative improvement of the formal errors of case 3 (a) and 4 (b) towards the EA scenario for a GRACE-type mission under consideration of the static gravity field signal and instrument errors assuming a 3D-hybridization.

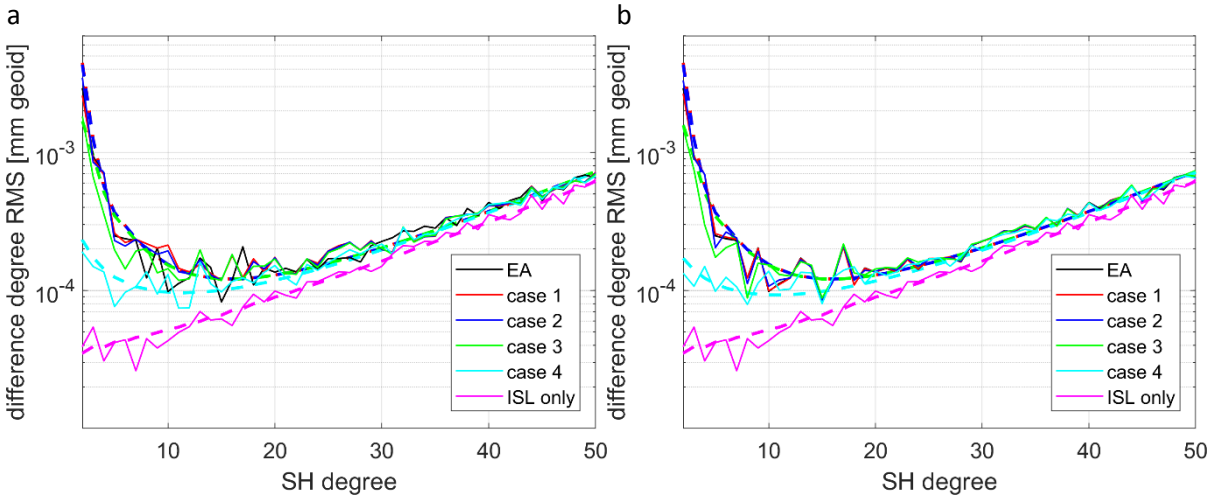

Figure 5. Degree RMS of residual coefficients for a Bender-type mission under consideration of the static gravity field signal and instrument errors assuming a 1D- (a) and a 3D-hybridization (b). The respective formal errors are shown as dashed lines of the corresponding colour.

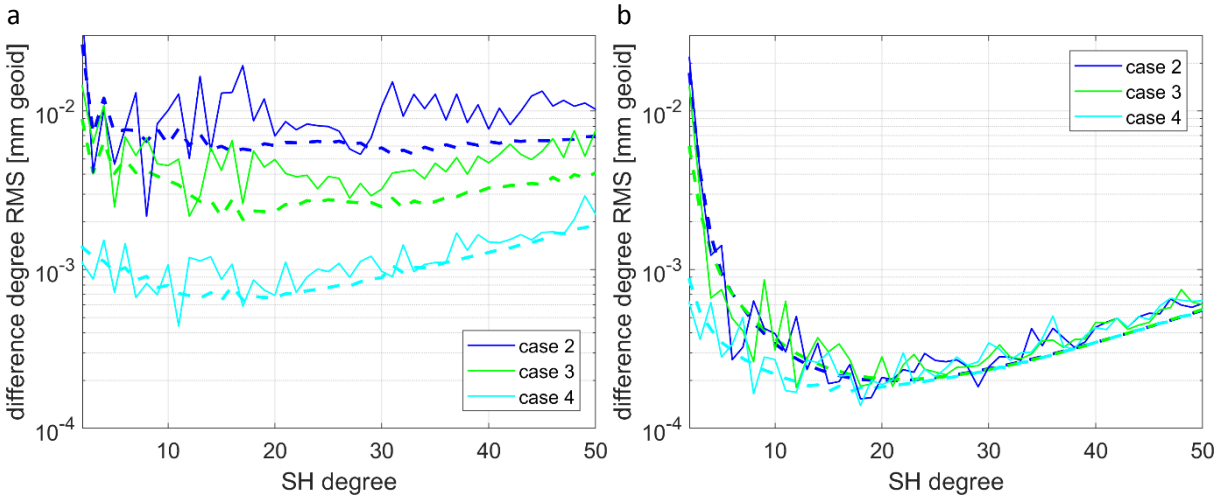

Figure 6. Degree RMS of residual coefficients obtained with the full-scale simulator for a GRACE-type (a) and a Bender-type (b) mission under consideration of the static gravity field signal and instrument errors assuming a 3D-hybridization. The respective formal errors are shown as dashed lines of the corresponding colour.

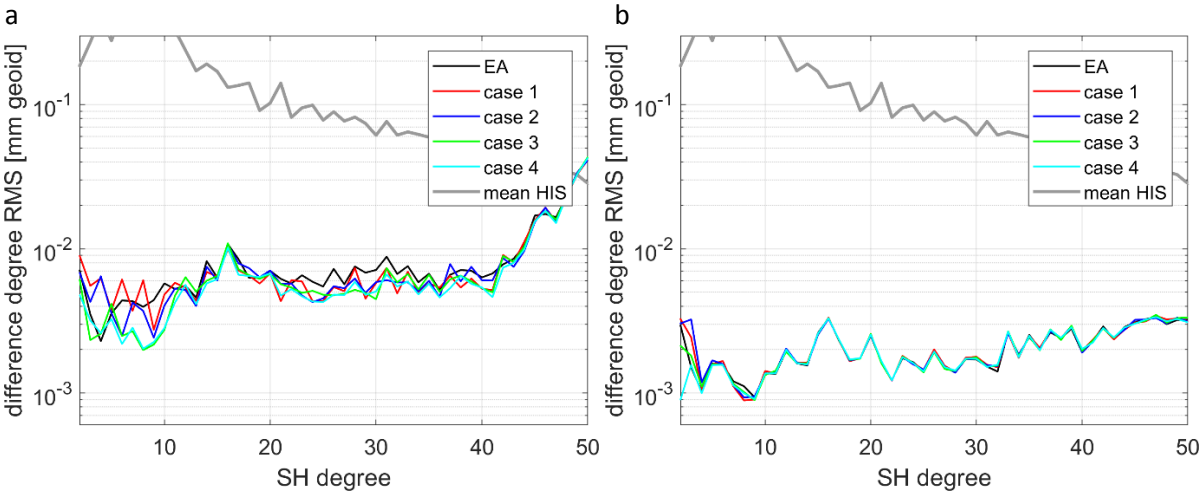

Figure 7. Degree RMS of residual coefficients for a GRACE-type (a) and Bender-type (b) mission under consideration of the static gravity field signal, its temporal variations induced by HIS and instrument errors assuming a 3D-hybridization.

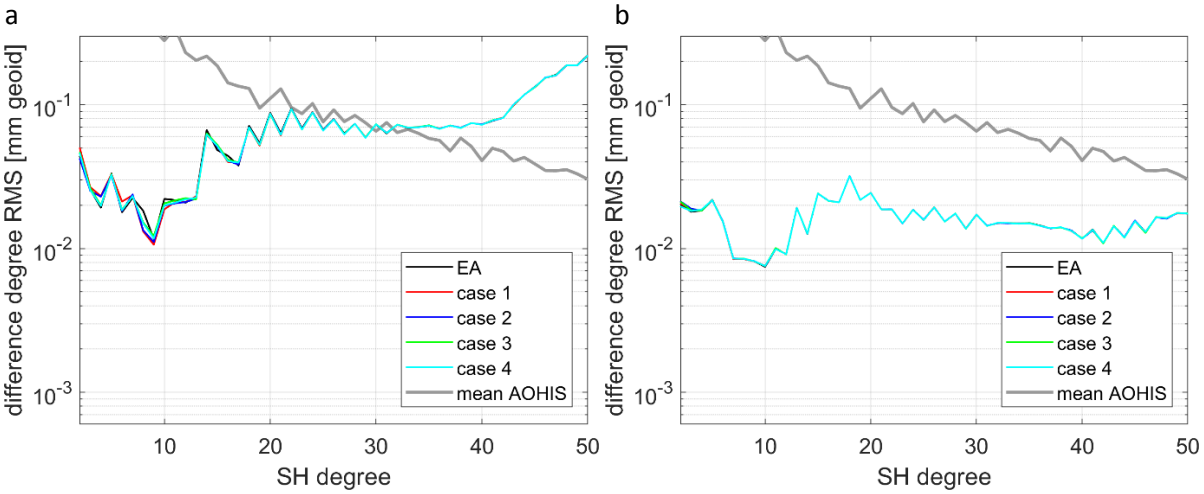

Figure 8. Degree RMS of residual coefficients for a GRACE-type (a) and Bender-type (b) mission under consideration of the static gravity field signal, its temporal variations induced by AOHIS and instrument errors assuming a 3D-hybridization.

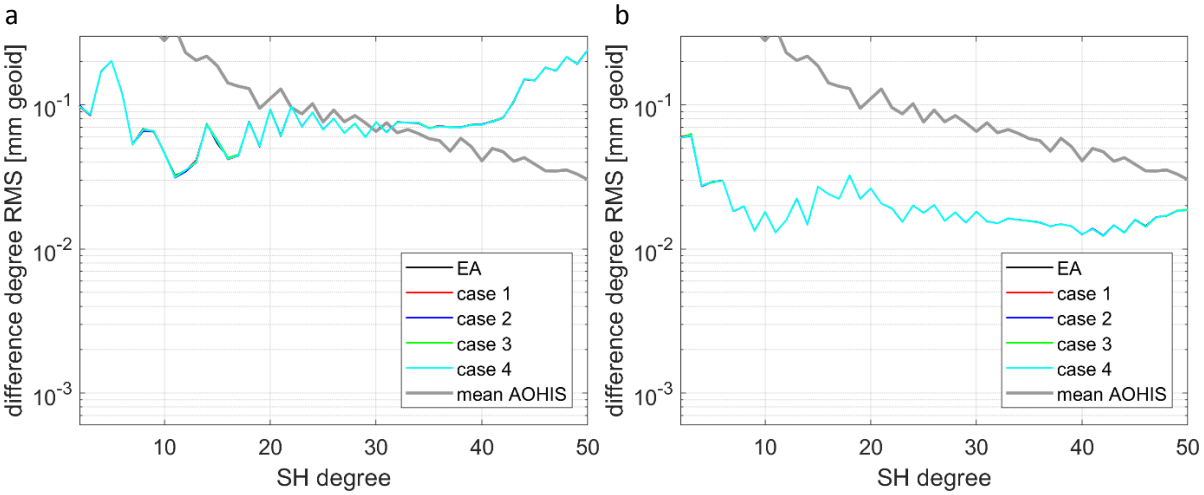

Figure 9. Degree RMS of residual coefficients for a GRACE-type (a) and Bender-type (b) mission under consideration of the static gravity field signal, its temporal variations induced by AOHIS as well as ocean tides and instrument errors assuming a 3D-hybridization.

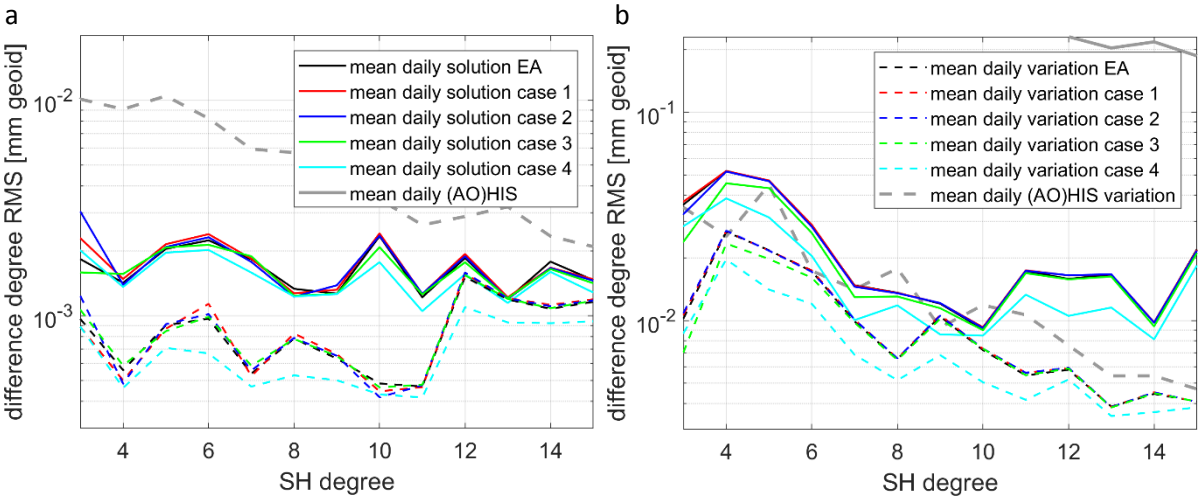

Figure 10. Degree RMS of residual coefficients of mean daily solutions (solid lines) as well as daily variations (dashed lines) obtained by Wiese parametrization of Bender-type-mission-based observations considering HIS- (a) and AOHIS-induced (b) temporal gravity field variations. A 3D-hybridization is assumed.

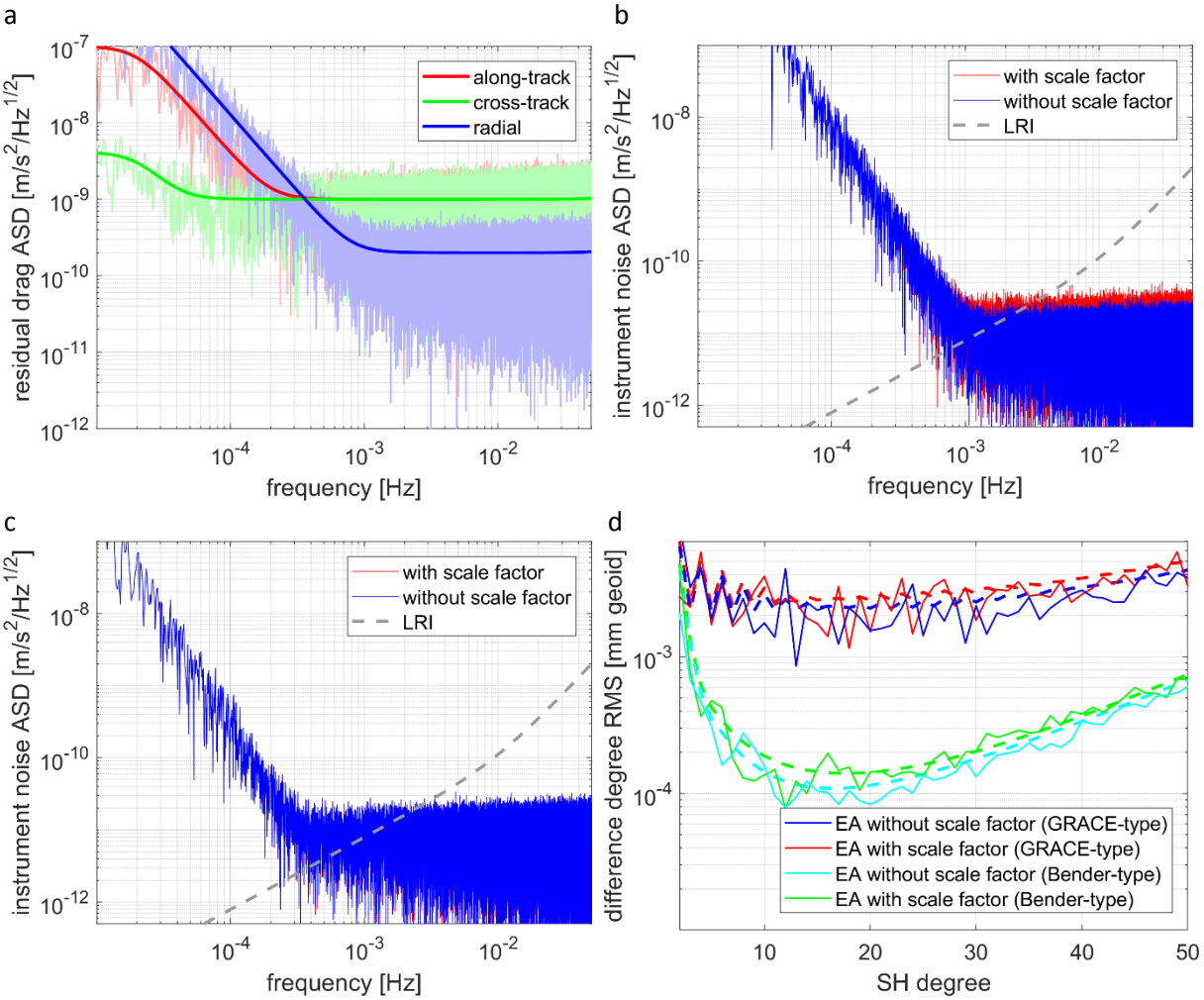

Figure 11. a) ASD of the residual drag specifications in along-track, cross-track and radial directions as specified in ESA's SC4MGV project; b) input accelerometer noise for the reduced-scale simulator in case of a standard EA with and without considering the scale factor (10^{-2} for every axis); c) input accelerometer noise for the reduced-scale simulator in case of case 4 assuming a 1D-hybridization with and without considering the scale factor (10^{-5} for along-track, 10^{-2} for cross-track and radial), d) Degree RMS of residual coefficients for a GRACE-type and Bender-type mission under consideration of the static gravity field signal and the standard EA instrument scenario with and without taking into account the scale factor according to b)